Regular Article

PHYSICAL CHEMISTRY RESEARCH
Published by the
Iranian Chemical Society
www.physchemres.org
info@physchemres.org

Phys. Chem. Res., Vol. 12, No. 2, 505-513, June 2024
DOI: 10.22036/pcr.2023.409079.2388

Photoluminescence Studies on Eu^{3+} Activated $Li_4Zn(PO_4)_2$ Phosphors

A. Naveen[a], M. Venkateswarlu[a,*], MVVK. Srinivas Prasad[a], N. Venkata Siva Krishna[b], G. Chandana[b], Y. Ramakrishna[b] and G. Giridhar[c,*]

[a]*Department of Engineering Physics, Koneru Lakshmaiah Education Foundation, Vaddeswaram, Guntur, A.P., India*
[b]*Department of Engineering Physics, AU College of Engineering (AUCE), Andhra University, Visakhapatnam, India*
[c]*Department of Nanotechnology, Acharya Nagarjuna University, Nagarjunanagar, A.P., India*
(Received 30 July 2023, Accepted 5 November 2023)

The combustion technique was used to successfully prepare new $Li_4Zn(PO_4)_2:Eu^{3+}$ orange-red phosphors. A detailed description of the crystal phase, size distribution, luminescence characteristics, and decay curves was provided. The P21(4) space group contributes to the monoclinic structure of the $Li_4Zn(PO_4)_2:Eu^{3+}$ phosphors. The existence of pure phases of the produced phosphors was confirmed by X-Ray diffraction analysis. The intense orange-red emission light that the $Li_4Zn(PO_4)_2:Eu^{3+}$ phosphors produce at 593 nm is attributable to the $^5D_0 \rightarrow {}^7F_1$ transitions. The placement of Eu^{3+} ions at various site symmetries is supported by the variation in the intensity of the electric and magnetic dipole transition. $Li_4Zn(PO_4)_2:xEu^{3+}$ was shown to perform best at a concentration of 0.1 mol%, which displays great color purity. All results indicate that the $Li_4Zn(PO_4)_2:xEu^{3+}$ phosphors have potential applications in W-LEDs.

Keywords: Photoluminescence, Phosphors, Phosphates, Orange-Red emission, Solid state lighting

INTRODUCTION

Solid-state lighting (SSL) based on light-emitting diodes (LEDs) is gaining in popularity due to its high energy efficiency, long lifetime, and environmental friendliness [1-5]. However, the color rendering index (CRI) of white LEDs based on blue LED chips and yellow phosphors is often insufficient, especially in the red spectral region. To improve the CRI of white LEDs, it is essential to develop new red or orange-red phosphors that can be efficiently excited by n-UV or blue LEDs [6,7]. Trivalent europium (Eu^{3+}) ions are promising candidates for use as red phosphors due to their characteristic red emission under UV light [8,9]. However, the emission intensity and color of Eu^{3+}-activated phosphors can be heavily influenced by the local environment of the Eu^{3+} ions [10-12]. Therefore, it is important to design phosphor hosts that can provide a suitable microenvironment for Eu^{3+} to achieve high emission efficiency and tunability in emission.

Phosphate phosphors are considered for use as luminous materials due to their low sintering temperature, high luminous efficiency, and high stability. Much research has been done on phosphors based on phosphate compounds with good thermal and hydrolytic stability because they are used in a wide variety of displays and illumination devices. Single-phase white lighting-emitting $Na_3Gd(PO_4)_2:Dy^{3+}$, Eu^{3+} phosphors exhibit high-intensity white light emission with energy transfer between activators upon n-UV excitation and have good thermal stability [13]. $CaSr_2(PO_4)_2:Eu^{3+}$ orthophosphate phosphors exhibit luminescence behavior suitable for non-contact optical thermometers and solid-state lighting sources [14]. Photoluminescence efficiency enhancement of Eu^{3+} has also been reported with the energy transfer mechanism from host to activator in various hosts [15-19]. Sahu *et al.* developed a glass-ceramic form of Eu^{3+}-

*Corresponding author. E-mail: drggiridhar@rediffmail.com, mvrmphil@gmail.com

doped phosphors and identified its sites [20]. Additionally, phosphors with Eu^{3+} have been reported for enhanced thermal stability and sensors [21-22].

In this communication, we report on the structural, morphological, elemental, and luminescent properties of Eu^{3+}-activated $Li_4Zn(PO_4)_2$ phosphors. We show that the Eu^{3+} emission intensity and color can be tuned by varying the Eu^{3+} concentration. We attribute this to the concentration-dependent changes in the local environment of the Eu^{3+} ions. Based on our findings, we confirm that $Li_4Zn(PO_4)_2$:Eu^{3+} is a tunable red phosphor for solid-state lighting with an enhanced color rendering index.

MATERIALS AND METHODS

$Li_4Zn(PO_4)_2$:xEu^{3+} (where x = 0.01, 0.03, 0.05, 0.08, and 0.1 mol%) phosphors were prepared by using combustion synthesis. High purity (99.9%) research-grade chemicals such as $LiNO_3$, $Zn(NO_3)_2$, and $(NH_4)H_2PO_4$ obtained from Loba Chemicals Pvt. Ltd.. India, and $Eu(NO_3)_3.6H_2O$ (99.99% ultra-pure) from SRL Pvt. Ltd.. India., used as starting materials. All precursors are taken in stoichiometric ratio along with urea as fuel and H_3BO_3 as flux. All the compounds were prepared in a systematic procedure [5,23]. The combustion reaction produced a white powder, which was ground to a fine powder. The powder was then characterized by X-Ray diffraction, energy dispersive spectroscopy, and photoluminescence spectroscopy. SHIMADZU LabX DRD-6100 diffractometer is used for X-Ray diffraction. Thermo Lumina spectrophotometer used to record photoluminescence spectra. Decay profiles were measured by using the Edinburgh Instruments FLSP 920 system. FTIR spectra were recorded by using BRUKER Alpha II in the range from 4000 cm^{-1} to 400 cm^{-1}. All the characterization is done at room temperature.

RESULTS AND DISCUSSION

Figure 1 depicts the X-Ray diffraction patterns of a new $Li_4Zn(PO_4)_2$ (pure) and doped (b) $Li_4Zn(PO_4)_2$: xEu^{3+} (where x= 0.01, 0.03, 0.05, 0.08 and 0.1) phosphors. The peaks were obtained and are in good agreement with the standard monoclinic structure of $Li_4Zn(PO_4)_2$ (JCPDS Card No. 01-73-0622). No other phases are seen dominantly suggesting the proper position of dopant ion in the host [9] and also evidences the production of high internal temperatures in the combustion method.

The high intense peak has been observed at $2\theta = 22.131^{o}$ corresponding to the (-1 1 2) plane. The crystallite sizes are calculated by using standard Debye-Scherrer's formula (Eq. (1))

$$D_{hkl} = \frac{0.9\,\lambda}{\beta Cos\theta} \quad (1)$$

where D-crystallite size, β-full width half maximum, λ– x-Ray wavelength. The calculated crystallite sizes are corresponding to the phosphors and are shown in Table 1.

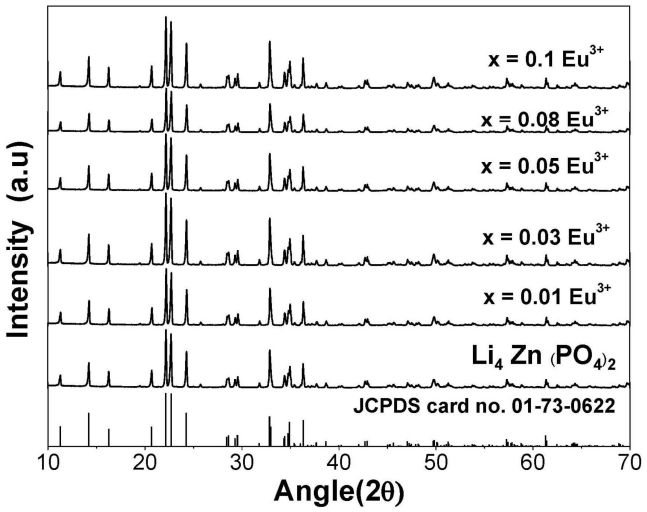

Fig. 1. X-Ray diffraction patterns of $Li_4Zn(PO_4)_2$:xEu^{3+} with standard structure.

Table 1. Crystallite Sizes from the X-Ray Diffraction Patterns for the Present Phosphors

Phosphor	Crystallite size (nm)
$Li_4Zn(PO_4)_2$-Pure	65.3
$Li_4Zn(PO_4)_2$:$0.01Eu^{3+}$	67.4
$Li_4Zn(PO_4)_2$:$0.03Eu^{3+}$	67.6
$Li_4Zn(PO_4)_2$:$0.05Eu^{3+}$	68.3
$Li_4Zn(PO_4)_2$:$0.08Eu^{3+}$	67.5
$Li_4Zn(PO_4)_2$:$0.1Eu^{3+}$	68.2

The crystallite size of the $Li_4Zn(PO_4)_2$ phosphors suggests the incorporation of Eu^{3+} ions in the host lattice and has no significant variations in crystallite sizes [24]. Except for small variations in peak intensities, no such other properties like broadening, large peak shifts were observed. The change in peak intensities is attributed to differences in electronic densities of the dopant and the host [25,26].

By using XRD software, the structure was refined with standard space group P21(4) and the monoclinic unit cell. The improved lattice parameters were determined to be as follows: cell volume V = 662.1912, a = 8.15635, b = 7.87928, c = 10.48591, beta = 100.69122. Inter planar distance - observed and calculated, along with full-width half maximum are shown in Table 1a.

Scanning Electron Microscope (SEM) images with EDS have been shown in Fig. 2. The images clearly show the agglomeration between the grains of the solid microcrystalline structures and irregular shapes which are attributed to high temperatures in combustion synthesis.

The lineal intercept technique is used to determine the average grain size (D) with the given equation is as follows [4,27].

$$D_{SEM} = \frac{1.56}{MN} \quad (2)$$

where L -length of grain, M-magnification, and N indicates the number of grain boundaries the lines intercept.

The average grain size of the un-doped and doped $Li_4Zn(PO_4)_2$ samples was determined to be 345 nm and 394 nm, respectively. The D_{SEM} values were discovered to be around 5-6 times greater than the D_{hkl} values. Here the average crystallite sizes determined by SEM profiles and XRD patterns are not the same due to their different evaluation parameters.

The presence of elements in $Li_4Zn(PO_4)_2$ phosphors was confirmed by energy dispersive X-Ray spectroscopy (EDS). The EDS lines for all elements except Li were monitored for the selected area, as the instrument is limited in its ability to detect light elements below carbon [10]. The EDS also showed that Eu is well-associated with Zn, which supports

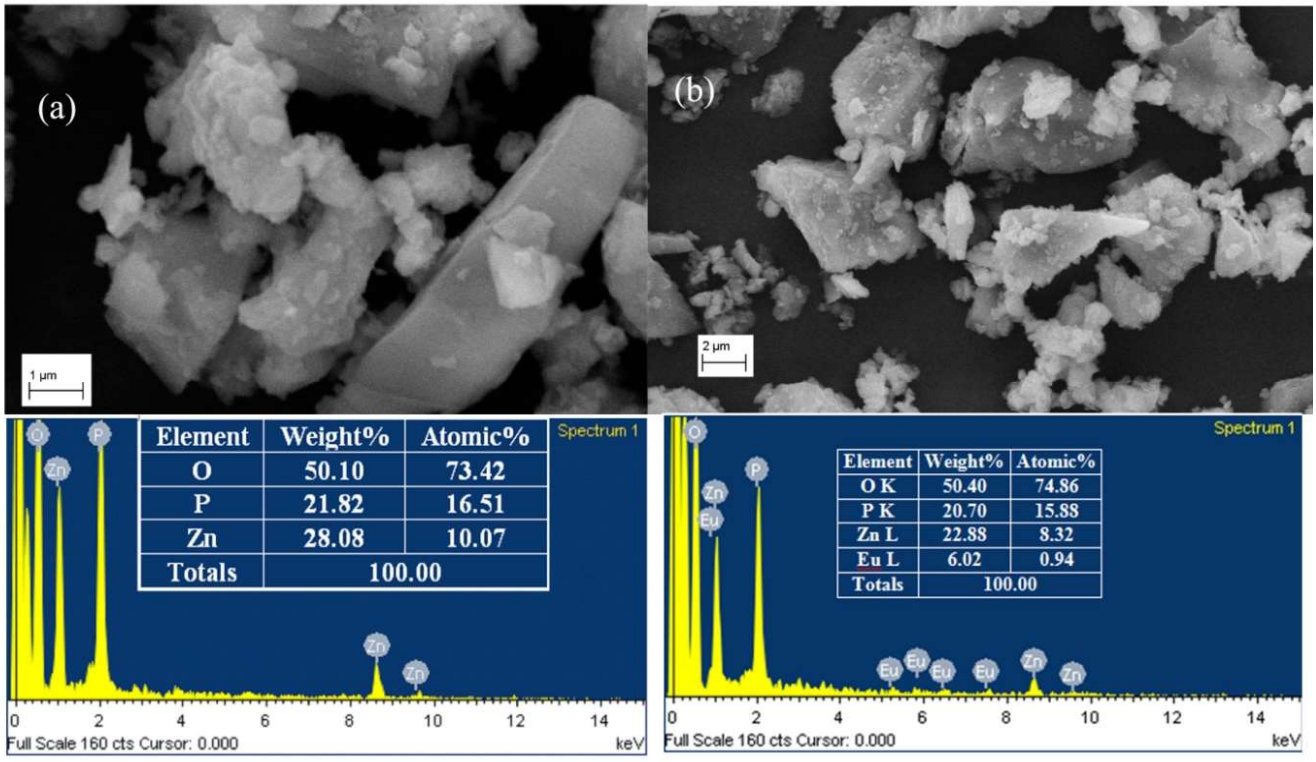

Fig. 2. SEM images and EDS details of pure $Li_4Zn(PO_4)_2$ and $Li_4Zn(PO_4)_2$:0.1Eu^{3+}.

the intensity variations in X-Ray diffraction patterns. Some additional peaks before oxygen in Fig. 2 also indicate the presence of oxygen, as its concentration is higher in the specimen.

The typical FTIR spectrum of $Li_4Zn(PO_4)_2$:xEu^{3+} phosphors is depicted in Fig. 3 in the 4000-550 cm^{-1} region. The FTIR spectrum shows signs of well-known phosphate vibrational bands. With dominating six bands at 568 cm^{-1}, 587 cm^{-1}, 601 cm^{-1}, 1000 cm^{-1}, 1216 cm^{-1}, and 1365 cm^{-1}, the spectra show nearly identical bond natures. The network of phosphate phosphors was established by the cross-linking PO_4 tetrahedra with terminal double-bonded oxygen and three bridging oxygen [28].

The bands assigned for the observed vibrations are ~$(PO_4)^{3-}$ for 568 and 587 cm^{-1} [29], $(P\text{-}O\text{-}P)_{sym}$ for 601cm^{-1}, $(PO_4)^{3-}$ for 1000 cm^{-1} [30], $(PO_2)_{as}$ vibration for 1215 cm^{-1} and P-O stretching of pyrophosphates for 1365 cm^{-1} [28,29,31] respectively.

The FTIR spectra of the synthesized phosphors show that the number and position of the bands have not changed significantly. However, there are some subtle changes, such as a relative increase in intensities and a slight shift in the bands. These changes are due to the incorporation of Eu^{3+} ions into the matrix, which results in the creation of non-bridging oxygen. The presence of non-bridging oxygen is characteristic of the phosphates family.

The excitation spectra of Eu^{3+} doped $Li_4Zn(PO_4)_2$ phosphors are shown in Fig. 4a. The spectrum shows six peaks in the region of 325 to 550 nm, which are due to 4f-4f electronic transitions [32,33]. These transitions are attributed to the Eu^{3+} ions transitioning from their ground state, $^7F_0$, to several excited states - $^5D_4$ (360 nm), $^5G_2$ (382 nm), $^5L_6$ (392 nm), $^5D_3$ (414 nm), $^5D_2$ (463 nm) and $^5D_1$ (531 nm). Due to the Eu^{3+} ion's $^7F_0 \rightarrow {}^5L_6$ (392 nm) transition, the highest excitation intensity peak is observed to be at 392 nm.

Figure 4b shows the emission spectrum of Eu^{3+} doped phosphors activated upon high intense excitation wavelength (λ_{ex} = 392 nm). The spectra revealed that the emission peaks of the Eu^{3+} ions observed in the host are at 593 nm, 612 nm, 652 nm, and 698 nm and the corresponding transitions from metastable state $^5D_0$ to - $^7F_1$, $^7F_2$, $^7F_3$ and $^7F_4$ respectively [9,32,34]. Here $^5D_0 \rightarrow {}^7F_2$ is the hypersensitive transition and its intensity varies with the Eu^{3+} local environment.

Eu^{3+} ions can be used to study the local structure and site

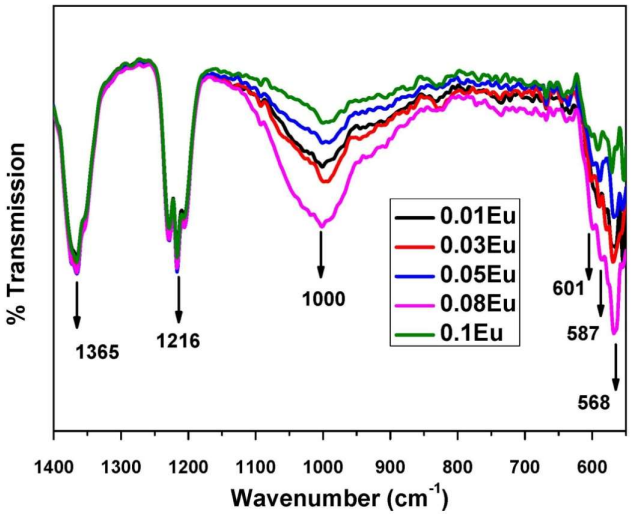

Fig. 3. FTIR spectra of $Li_4Zn(PO_4)_2$: x Eu^{3+} phosphors.

symmetry of their host materials. The intensity ratio of the electric dipole (ED) $^5D_0 \rightarrow {}^7F_2$ transition to the magnetic dipole (MD) $^5D_0 \rightarrow {}^7F_1$ transition in the excitation and emission spectra of Eu^{3+} ions is sensitive to the local environment around the dopant ion, especially the symmetry of the first coordination shell [20]. In an asymmetric environment, the ED transition will be more intense than the MD transition, and vice versa in a symmetric environment. The MD transition $^5D_0 \rightarrow {}^7F_1$ has an orange emission (590-600 nm) and is not strongly influenced by the local site symmetry, while the ED transition $^5D_0 \rightarrow {}^7F_2$ has a red emission (~610-630 nm) and is highly sensitive to the local site symmetry of the Eu^{3+} ion. For Eu^{3+} concentrations of 0.01, 0.03, and 0.05 mol%, the ED transition at 612 nm ($^5D_0 \rightarrow {}^7F_2$) is stronger than the MD transition at 593 nm ($^5D_0 \rightarrow {}^7F_1$). This suggests that the Eu^{3+} ions are located at highly asymmetric sites, where their intensities are strongly influenced by the environment around them [35]. At Eu^{3+} concentrations of 0.08 and 0.1 mol%, the MD transition is dominant over the ED transition. This suggests that the Eu^{3+} ions are located at symmetric sites, where the intensity is not affected by the local crystal field around the Eu^{3+} ion. However, the Eu^{3+} ions are still not in perfect symmetry sites, as there has been a slight change in their coordination in the host related to its concentration. If the Eu^{3+} ions were in perfect symmetry sites, the ED transitions would be absent. However, this has not happened in this host, except that the

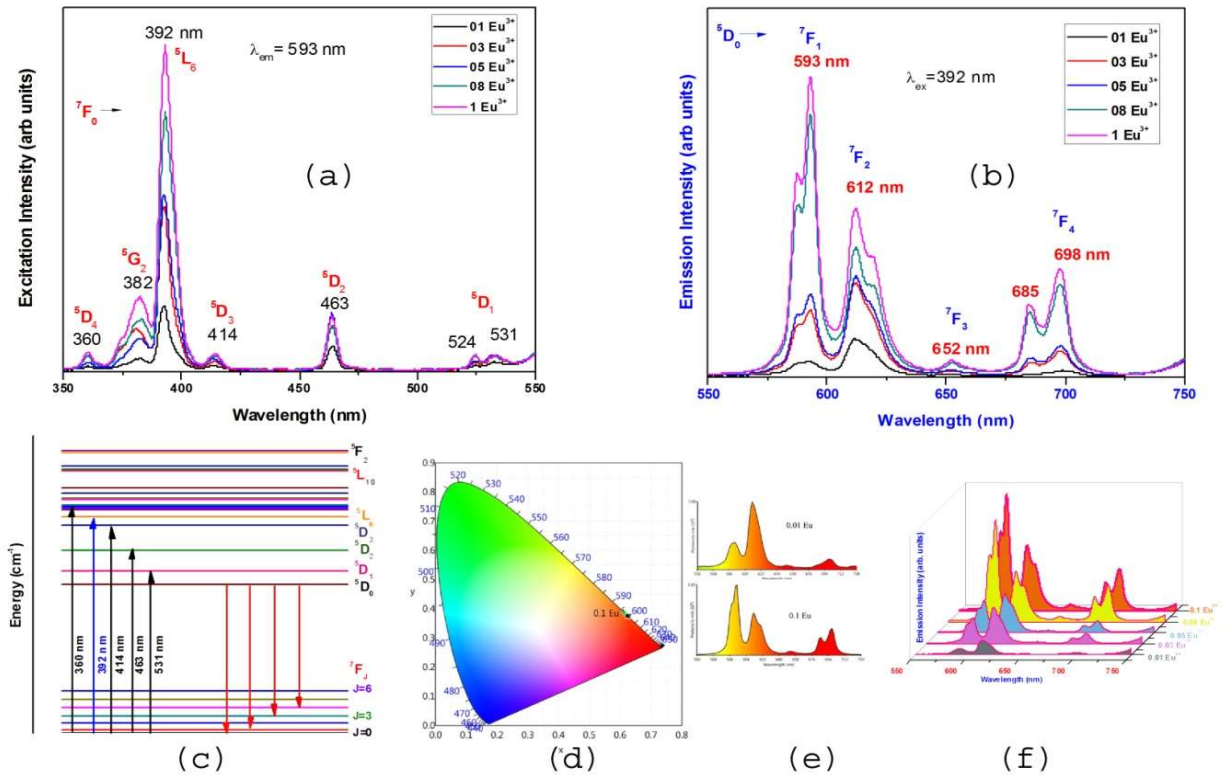

Fig. 4. Photoluminescence mechanism of $Li_4Zn(PO_4)_2$: Eu^{3+} phosphors [(a) Emission spectra, (b) Excitation spectra (c) energy level diagram (d) Chromaticity diagram (e) (f) variation in emission intensities at different concentrations].

reduction in ED transition intensity may suggest a change in its coordination. Thus, in addition to its orange-red emission, which has applications in phosphor materials, the sensitivity of the Eu^{3+} ion to the local site in the host matrix is extensively used as a local structure probe [36]. The relative intensity of the ED and MD lines also determines the final emission color of the samples and leads to the tuning in emission.

Therefore tuning of emission by Eu^{3+} concentration [37] is possible because of the existence of dopant ions with both asymmetric and symmetric character in one host. This could explain the importance of concentration variation of dopants in phosphors for various optical applications. The decreasing intensity at higher concentrations is due to energy transfer to non-radiative centers as the distance between Eu^{3+} ions decreases [38].

The decay profiles of the phosphors were investigated at a wavelength of 612 nm (λ_{em}) under excitation at 392 nm (λ_{ex}). The lifetime decay values were calculated using the first-order exponential decay function. Fig.5 shows that the lifetime decreases with increasing Eu^{3+} concentration in the phosphors. This suggests that defects are created within the sub-lattice at higher concentrations. The lifetime decay values for 0.01, 0.03, 0.05, 0.08, and 0.1 mol% of Eu^{3+} are 1.832, 1.83, 1.826, 1.825, and 1.821 milliseconds, respectively. This range of lifetimes suggests that the probability of energy transfer between the host and activator ions is reduced. The energy level diagram in Fig. 4c shows the electronic transitions of Eu^{3+} ions in the present host. The Eu^{3+} ions are excited from the lower level ($^7F_0$) to the higher level ($^5L_6$) and then de-excited from the higher levels ($^5D_0$) to the lower levels ($^7F_{1,2,3,4}$). There are also non-radiative transitions ($^5L_6 \rightarrow {}^5D_{3,2,1,0}$) that occur.

The performance of the prepared phosphors is estimated by the CIE 1931 (Commission Internationale de I'Eclairage) color coordinates (x,y) by using Eq. (2) from the tri-stimulus values.

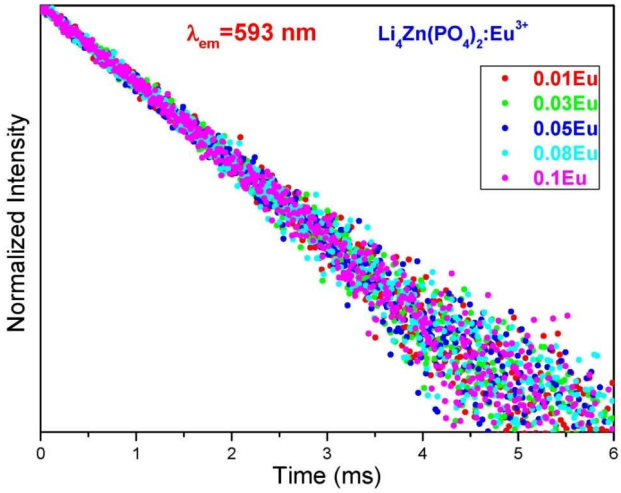

Fig. 5. Decay profiles of Eu^{3+} doped $Li_4Zn(PO_4)_2$ phosphors.

$$x = \frac{X}{X+Y+Z} \tag{2a}$$

$$y = \frac{Y}{X+Y+Z} \tag{2b}$$

Where *X, Y,* and *Z* are the colour-matching functions for primary red, green, and blue colors to match the color of $P(\lambda)$. The color-matching functions can be evaluated using the following equations [39]

$$X = \int_{\lambda} \bar{x}(\lambda) P(\lambda) d\lambda \tag{3a}$$

$$Y = \int_{\lambda} \bar{y}(\lambda) P(\lambda) d\lambda \tag{3b}$$

$$Z = \int_{\lambda} \bar{z}(\lambda) P(\lambda) d\lambda \tag{3c}$$

CIE chromaticity diagram of Eu^{3+} doped $Li_4Zn(PO_4)_2$ phosphors are shown in Fig. 8. Further, color purity is also an important parameter which is estimated using Eq. (4) with (x,y) color coordinates and standard values. The expression to evaluate the color purity is:

$$\text{Color purity} = \frac{\sqrt{(x-x_{ee})^2 + (y-y_{ee})^2}}{\sqrt{(x_d-x_{ee})^2 + (y_d-y_{ee})^2}} \tag{4}$$

where $(x, y), (x_{ee}, y_{ee})$ are the chromaticity coordinates of the emission light and equal energy point and (x_d, y_d) are the dominant wavelength points.

Color Calculator v7.77 software is used to evaluate the aforesaid photometric parameters. It was observed that all the CIE color coordinates lie in the orange-red region [38-40] and the other evaluated parameters are presented in Table 2. All the coordinates are well placed and the inset shows the change in intensity of 0.01 and 0.1 mol% samples. The CCT values and color purity depend on both the dopant concentration and excitation wavelength [40,41]. The obtained values for the $Li_4Zn(PO_4)_2$:xEu^{3+} with other parameters are in correlation to orange-red light [9,12,42].

Overall, the studies reveal the present $Li_4Zn(PO_4)_2$ host is a suitable candidate for accepting rare earth ions with and without crystal field effects. So, this kind of single-phased hosts are very useful in the fabrication of display and lighting devices.

CONCLUSION

$Li_4Zn(PO_4)_2$:xEu^{3+} phosphors (where 0.01 < x < 0.1) were synthesized using the combustion synthesis method.

Table 2. CIE Chromaticity Coordinates for $Li_4Zn(PO_4)_2$ Phosphor

Sample	x	y	Lumens 10^{-20}	Visible power (mW) 10^{-20}
0.01 Eu^{3+}	0.6249	0.3746	2.2	6.8
0.03 Eu^{3+}	0.6248	0.3747	5.8	18
0.05 Eu^{3+}	0.6234	0.3762	6.7	21
0.08 Eu^{3+}	0.6097	0.3898	13	41
0.1 Eu^{3+}	0.6125	0.3870	16	50

The structure, phase, and elemental composition of the phosphors were investigated using XRD and SEM. The results showed that the phosphors are uniform and have excellent crystallinity. The FTIR spectrum showed the fundamental vibrations of the phosphate unit. All of the prepared phosphors emit red light by radiative transitions from the $^5D_0$ level to the $^7F_{1,2,3, \text{ or } 4}$ levels upon excitation. The nature of the emission (symmetric or asymmetric) depends on the Eu^{3+} concentration and the dominant magnetic dipole or electric dipole interactions. The color temperature and color purity values showed a good red warm light, and the CIE coordinates were well positioned in the orange-red region. The results indicate that the synthesized $Li_4Zn(PO_4)_2:xEu^{3+}$ phosphors are suitable candidates for use in white LEDs and photoluminescent display devices.

REFERENCES

[1] Daicho, H.; Iwasaki, T.; Enomoto, K.; Sasaki, Y.; Maeno, Y.; Shinomiya, Y.; Aoyagi, S.; Nishibori, E.; Sakata, M.; Sawa, H., *et al.* A Novel Phosphor for Glareless White Light-Emitting Diodes. *Nat. Commun.* **2012**, *3*, 1132, DOI: 10.1038/ncomms2138.

[2] Pust, P.; Schmidt, P. J.; Schnick, W., A Revolution in Lighting. *Nat. Mater.* **2015**, *14*, 454-458, DOI: 10.1038/nmat4270.

[3] Butler, K. H., Improved Calcium Halo-Phosphate Phosphor 1951, https://patents.google.com/patent/US2579900A/en

[4] Yawalkar, M. M.; Zade, G. D.; Singh, V.; Dhoble, S. J., Investigation of Luminescence Processes in $Li_6Gd(BO_3)_3:Eu^{3+}$ Phosphor. *J. Mater. Sci. Mater. Electron.* **2017**, *28*, 180-189, https://doi.org/10.1007/s10854-016-5509-y

[5] Shinde, K. N., Dhoble, S. J., Swart, H. C., Park, K., *Introduction. In: Phosphate Phosphors for Solid-State Lighting.*; 2013; Vol. 174; ISBN 978-3-642-33450-4, https://doi.org/10.1007/978-3-642-34312-4_8

[6] Lin, Y. S.; Jheng, D. Y.; Hsu, K. Y.; Tsai, C. N.; Huang, S. L., Ce^{3+}, Sm^{3+}: YAG Double Clad Crystal Fiber Broadband Light Source. In Proceedings of the CLEO: Science and Innovations; Optical Society of America, 2011, p. CTuI7, https://doi.org/10.1364/CLEO_SI.2011.CTuI7.

[7] Li, K.; Deun, R., Photoluminescence and Energy Transfer Properties of a Novel Molybdate $KBaY(MoO_4)_3:Ln^{3+}$(Ln^{3+} = Tb^{3+}, Eu^{3+}, Sm^{3+}, Tb^{3+}/Eu^{3+}, Tb^{3+}/Sm^{3+}) as a Multi-Color Emitting Phosphor for UV w-LEDs. *Dalton Trans.* **2018**, *47*, DOI: 10.1039/C8DT01011K.

[8] Fan, G.; Wang, L.; Hu, R.; Fan, D., A White LED with Orange-Red Phosphors $KBaBP_2O_8:Eu^{3+}$. *Inorg. Chem. Commun.* **2021**, *127*, 108527, https://doi.org/10.1016/j.inoche.2021.108527.

[9] Ravi, M.; Chakrapani, G. P.; Mahitha, B., Photoluminescence Studies on $LiNa_5(PO_4)_2$: Eu^{3+} Phosphor. *Bioint. Res. Appl. Chem.* **2022**, https://doi.org/10.33263/BRIAC132.175.

[10] Munirathnam, K.; Dillip, G. R.; Raju, B.; Joo, S. W.; Dhoble, S. J.; Nagabhushana, B. M.; Hari Krishna, R.; Ramesh, K. P.; Varadharaj Perumal, S.; Prakashbabu, D., Synthesis, Photoluminescence and Judd-Ofelt Parameters of $LiNa_3P_2O_7$: Eu^{3+} Orthorhombic Microstructures. *Appl. Phys. A* **2015**, *120*, 1615-1623, https://doi.org/10.1007/s00339-015-9371-1.

[11] An, J.; Zhang, Z.; Qiu, Y.; Fu, Z.; Zhou, Y.; Zeng, F., Luminescence Properties of Borosilicate Glass Doped with $Ce^{3+}/Dy^{3+}/Eu^{3+}$ under Ultraviolet Excitation for White LED. *J. Non-Cryst. Solids* **2019**, *503*, 208-213, https://doi.org/10.1016/j.jnoncrysol.2018.09.050.

[12] Babu, P. R.; Gelija, D.; Pasupuleti, K. S.; Kumar, B. K.; Sushma, N. J.; Kim, M. -D.; Raju, B. D. P., Optical, Emission, and Excitation Dynamics of Eu^{3+}-Doped Bismuth-Based Phosphate Glass for Visible Display Laser Applications. *Luminescence* **2023**, *38*, 71-82, https://doi.org/10.1002/bio.4422.

[13] Xie, M.; He, C.; Fang, M.; Huang, Z.; Liu, Y.; Wu, X.; Min, X., Improvement of Luminescence Performance of Single-Phase White-Emitting $Na_3Gd(PO_4)2:Dy^{3+}$ Phosphor by Co-Doping with Eu^{3+}. *Polyhedron* **2022**, 115860, https://doi.org/10.1016/j.poly.2022.115860.

[14] Singh, R.; Manhas, M.; Bedyal, A. K.; Durani, F.; Swart, H. C.; Kumar, V., Thermometric and Luminescence Studies of Eu^{3+} Activated $CaSr_2(PO_4)_2$ Phosphor for Non-Contact Optical Thermometry and Solid State Lighting Applications. *Mater. Chem. Phys.* **2022**, *291*, 126735, https://doi.org/10.1016/j.matchemphys.2022.126735.

[15] Singh, S. P.; Karmakar, B., Photoluminescence Enhancement of Eu^{3+} by Energy Transfer from Bi^{2+} to Eu^{3+} in Bismuth Glass Nanocomposites. *RSC Adv.* **2011**, *1*, 751-754, https://doi.org/10.1039/C1RA00160D.

[16] Deshmukh, R. G.; Kadam, A. R.; Dhoble, S. J., Energy Transfer Mechanism in $K_2Ba(PO_4)F:Dy^{3+},Eu^{3+}$ Co-Activated Phosphor: Spectral Tuning Phosphor for Photovoltaic Efficiency Enhancement. *J. Mol. Struct.* **2022**, *1257*, 132603, DOI: 10.1016/j.molstruc.2022.132603.

[17] Anilkumar, K.; Damodaraiah, S.; Babu, S.; Prasad, V. R.; Ratnakaram, Y. C., Emission Spectra and Energy Transfer Studies in Dy^{3+} and Dy^{3+}/Eu^{3+} Co-Doped Potassium Fluorophosphate Glasses for White Light Applications. *J. Lumin.* **2019**, *205*, 190-196, https://doi.org/10.1016/j.jlumin.2018.09.007.

[18] Bosze, E. J.; Hirata, G. A.; Shea-Rohwer, L. E.; McKittrick, J., Improving the Efficiency of a Blue-Emitting Phosphor by an Energy Transfer from Gd^{3+} to Ce^{3+}. *J. Lumin.* **2003**, *104*, 47-54, https://doi.org/10.1016/S0022-2313(02)00663-4.

[19] Evaluating Thermal Quenching Temperature in Eu^{3+}-Substituted Oxide Phosphors *via* Machine Learning ACS Applied Materials & Interfaces Available online: https://pubs.acs.org/doi/10.1021/acsami.9b16065 (accessed on 30 April 2023).

[20] Sahu, M.; Phatak, N.; Saxena, M. K., Exploring Color Tunable Emission Characteristics of Eu^{3+} Doped $La_2(MoO_4)_3$ Phosphors in the Glass-Ceramic Form. *RSC Adv.* **2021**, *11*, 17488-17497. https://doi.org/10.1039/D1RA01715B.

[21] Novel and Wide-Ranging Color Tuning Photoluminescence Properties of Tb^{3+}/Eu^{3+} Doped Garnet-Type $Li_3Lu_3Te_2O_{12}$ Phosphor: Energy Transfer and Enhanced Thermal Stability-ScienceDirect Available online: https://www.sciencedirect.com/science/article/pii/S0925838821009154?via%3Dihub (accessed on 30 April 2023).

[22] Song, M.; Ran, W.; Ren, Y.; Wang, L.; Zhao, W., Characterizations and Photoluminescence Properties of a Dual-Functional $La_2LiNbO_6:Bi^{3+},Eu^{3+}$ Phosphor for WLEDs and Ratiometric Temperature Sensing. *J. Alloys Compd.* **2021**, *865*, 158825, DOI: 10.1016/j.jallcom.2021.158825.

[23] Ravi, M.; Chakrapani, G. P.; Balachandrika, M.; Vasudevarao, P.; Nageswararao, C.; Babu, L. K. K.; Prasad, P. M.; Giridhar, G., Photoluminescence Studies on $LiNa_5(PO_4)_2$: Dy^{3+},Sm^{3+} Phosphor. *Z. Für Naturforschung A* **2021**, https://doi.org/10.1515/zna-2021-0153.

[24] Indumathi, K.; Tamilselvan, S.; Rajasekaran, L.; David, A. D. J.; Muhammad, G. S.; Ramalingam, G.; Biruntha, M., Structural and Optical Properties of Eu^{3+} Doped Sr_3Gd $[PO_4]_3$ Phosphor White-LED Application. *Mater. Lett.* **2022**, *309*, 131371, https://doi.org/10.1016/j.matlet.2021.131371.

[25] Meetei, S. D.; Singh, S. D., Effects of Crystal Size, Structure and Quenching on the Photoluminescence Emission Intensity, Lifetime and Quantum Yield of ZrO_2: Eu^{3+} Nanocrystals. *J. Lumin.* **2014**, *147*, 328-335. https://doi.org/10.1016/j.jlumin.2013.11.064 .

[26] Revathy, J. S.; Priya, N. S. C.; Sandhya, K.; Rajendran, D. N., Structural and Optical Studies of Cerium Doped Gadolinium Oxide Phosphor. *Bull. Mater. Sci.* **2021**, *44*, 13, DOI: 10.1007/s12034-020-02299-w.

[27] Wurst, J. C., Linear Intercept Technique for Measuring Grain Size in Two-Phase Polycrystalline Ceramics. *J. Am. Ceram. Soc.* **1972**, *55*, 109, https://doi.org/10.1111/j.1151-2916.1972.tb11224.x.

[28] Raynaud, S.; Champion, E.; Bernache-Assollant, D.; Thomas, P., Calcium Phosphate Apatites with Variable Ca/P Atomic Ratio I. Synthesis, Characterisation and Thermal Stability of Powders. *Biomaterials* **2002**, *23*, 1065-1072, https://doi.org/10.1016/S0142-9612(01)00218-6.

[29] Destainville, A.; Champion, E.; Bernache-Assollant, D.; Laborde, E., Synthesis, Characterization and Thermal Behavior of Apatitic Tricalcium Phosphate. *Mater. Chem. Phys.* **2003**, *80*, 269-277, https://doi.org/10.1016/S0254-0584(02)00466-2.

[30] Patel, N. P.; Srinivas, M.; Verma, V.; Modi, D., The Effect of $Tb3^+$ on α-$Sr_2P_2O_7$ Phosphor for Green LED Phosphor Application. In Proceedings of the AIP Conference Proceedings; AIP Publishing LLC, **2015**, *1665*, 110017, https://doi.org/10.1063/1.4918073.

[31] Zhang, Z.; Wu, Y.; Shen, X.; Ren, Y.; Zhang, W.; Wang, D., Enhanced Novel Orange Red Emission in $Ca_3(PO_4)_2:Sm^{3+}$ by Charge Compensation. *Opt. Laser Technol.* **2014**, *62*, 63-68, https://doi.org/10.1016/j.optlastec.2014.02.014.

[32] Meena, M. L.; Lu, C. -H.; Som, S.; Chaurasiya, R.; Lin, S. D., Highly Efficient and Thermally Stable Eu^{3+} Activated Phosphate Based Phosphors for WLEDs: An Experimental and DFT Study. *J. Alloys Compd.* **2022**, *895*, 162670, https://doi.org/10.1016/j.jallcom.2021.162670.

[33] Jayachandiran, M.; Annadurai, G.; Kennedy, S. M. M., Photoluminescence Properties of Red Emitting $Ba_3Bi_2(PO_4)_4$: Eu^{3+} Phosphor for WLEDs Applications. *J. Lumin.* **2018**, *201*, 196-202, https://doi.org/10.1016/j.jlumin.2018.04.054.

[34] Cao, R.; Zheng, Y.; Chen, T.; Lan, B.; Li, L.; Zhong, Q.; Nie, S.; Wang, J., Synthesis and Tunable Emission from Yellow-Green to Red-Orange of $Ca_3MgSi_2O_8$: Eu^{3+}, Dy^{3+} Phosphor. *J. Mol. Struct.* **2022**, *1262*, 133008, https://doi.org/10.1016/j.molstruc.2022.133008.

[35] Phatak, R.; Pathak, N.; Muhammed, S.; Sali, S. K.; Das, A., Crystal Structure and Site Symmetry of Undoped and Eu^{3+} Doped Ba_2LaSbO_6 and $BaLaMSbO_6$ Compounds (M = Mg,Ca): Tuning Europium Site Occupancy to Develop Orange and Red Phosphor. *Chem. Plus. Chem.* **2018**, *83*, 1144-1152, DOI: 10.1002/cplu.201800514.

[36] Phatak, R.; Pathak, N.; Muhammed, S.; Das, A.; Sali, S. K., Probing Crystal Structure and Site-selective Photo-physical Properties of Various Eu^{3+} -doped Niobates. *J. Am. Ceram. Soc.* **2020**, *103*, 2617-2629, DOI: 10.1111/jace.16953.

[37] Zhang, J.; Cai, G.; Wang, W.; Ma, L.; Wang, X.; Jin, Z., Tuning of Emission by Eu^{3+} Concentration in a Pyrophosphate: The Effect of Local Symmetry. *Inorg. Chem.* **2020**, *59*, 2241-2247, DOI: 10.1021/acs.inorgchem.9b02949.

[38] Vimal, G.; Mani, K. P.; Biju, P. R.; Joseph, C.; Unnikrishnan, N. V.; Ittyachen, M. A., Structural Studies and Luminescence Properties of $CeO_2:Eu^{3+}$ Nanophosphors Synthesized by Oxalate Precursor Method. *Appl. Nanosci.* **2015**, *5*, 837-846, DOI: 10.1007/s13204-014-0375-5.

[39] Schubert, E. F.; Kim, J. K., Solid-State Light Sources Getting Smart. *Science* **2005**, *308*, 1274-1278, https://doi.org/10.1126/science.1108712.

[40] Hakeem, D. A.; Pi, J. W.; Jung, G. W.; Kim, S. W.; Park, K., Structural and Photoluminescence Properties of $La_{1-X}NaCaGa_3PZrO_{12}$ Doped with Ce^{3+}, Eu^{3+}, and Tb^{3+}. *Dyes Pigments* **2019**, *160*, 234-242, https://doi.org/10.1016/j.dyepig.2018.06.047.

[41] Hakeem, D. A.; Pi, J. W.; Kim, S. W.; Park, K., Inorganic Chemistry Frontiers C8qi00111a, https://doi.org/10.1039/C8QI00111A.

[42] Ci, Z.; Sun, Q.; Qin, S.; Sun, M.; Jiang, X.; Zhang, X.; Wang, Y., Warm White Light Generation from a Single Phase Dy^{3+} Doped $Mg_2Al_4Si_5O_{18}$ Phosphor for White UV-LEDs. *Phys. Chem. Chem. Phys.* **2014**, *16*, 11597-11602, DOI: 10.1039/c4cp00357h.